



ANALYSIS OF THE JET NOISE EMITTED BY AN AIRCRAFT DURING TAKE-OFF

Henri Siller, Timo Schumacher, and Wolfram Hage

German Aerospace Center (DLR), Institute of Propulsion Technology, Engine Acoustics Department
Müller-Breslau-Str. 8, 10623 Berlin, Germany

Abstract

Microphone array measurements with the DLR research aircraft ATRA flying in different configurations are presented with a focus on the analysis of sources in the engine jets. The free jets exiting the engine nozzles are large distributed source regions with locally and temporally fluctuating source distributions that evolve in the downstream direction. The source maps from the array data calculated with a deconvolution method for moving sources are divided into integration regions for the different noise sources of the engine and the free jet downstream. Frequency spectra of the integrated noise powers from the source regions of the engine inlets, the nozzles, and the jets for fly-overs in three different configurations with high engine speeds are presented and compared.

1 INTRODUCTION

DLR performed flyover measurements with its research aircraft ATRA within the framework of the research project LNATRA. The purpose of these experiments was to test different noise reduction modifications on the aircraft in flight. This paper is focused on the results of the experiments with the ATRA in its baseline configuration for flight configurations corresponding to take-off and cut-back that were analysed with a focus on the contribution of jet noise. The ATRA is an Airbus A320 with V2500 engines, which in its baseline configuration features the vortex generators underneath the wings that inhibit the generation of aeolian tones at the over-pressure valve openings that used to be the signature tone of the A319/20 fleet. While the experiments are part of the DLR project LNATRA, the work on the analysis method is connected to the EU project ADEC[4].

The fly-over measurements were performed at the Cochstedt airfield near Magdeburg, Germany in May 2016. Some results from the 2016 fly-over measurements with the ATRA have already been presented at the 2018 BeBeC [7].



Figure 1: Left: The microphone array with the ATRA in the background. Right: The ATRA flying over the microphone array.

2 EXPERIMENTS

For the fly-over experiments, the aircraft was repeatedly flown over the array in different configurations, such that every configuration was repeated several times and on different days with different ambient conditions.

The microphone array consisted of 238 microphones that were distributed over an area of 35 by 40 m. They were arranged in a logarithmic spiral that was stretched in the direction of flight and offset from the runway centre line by 8 m. A schematic of the microphone arrangement is shown in figure 2 together with a photo of the array.

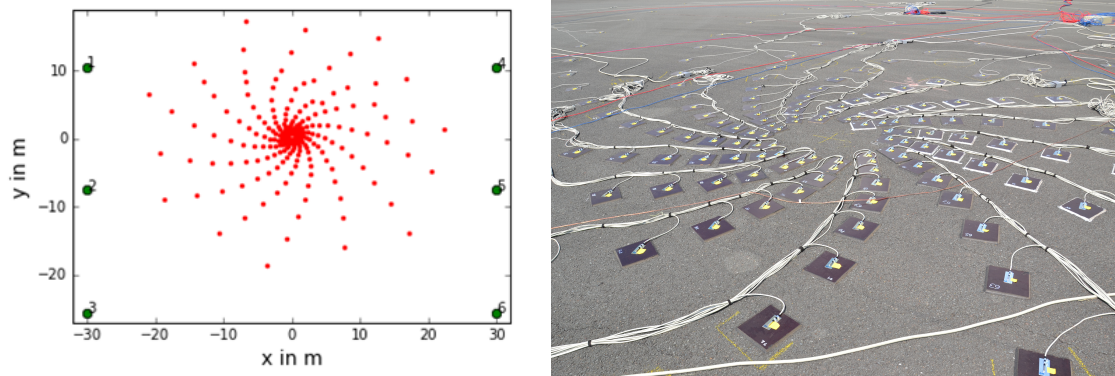


Figure 2: Left: Schematic of the arrangements of microphones (red dots) and laser distance meters (green dots) in the microphone array. Right: The center region of the microphone array.

The data of the 238 microphones were recorded with a sampling frequency of 48 kHz together with the signals from an array of laser distance meters that generated trigger signals when the aircraft passed overhead and with data from a GPS time-code generator for the later synchronisation with flight log data from the aircraft. The aircraft flight log and the trigger times and altitudes measured with an array of laser distance meters on the ground were used to approximate the aircraft trajectory parameters ground speed, vertical speed and altitude.

Config	Record	N1 in %	U_f in m/s	U_j in m/s	a in m/s	U_w in kts	M_j —	M_f —	$M_j - M_f$ —
1	REC135	79.8	70.9	289.2	340.8	3.1	0.85	0.21	0.64
2	REC005	90.6	77.6	343.8	344.1	9.7	1.00	0.23	0.77
2	REC136	90.0	67.2	339.4	340.6	2.9	1.00	0.20	0.80
3	REC022	81.0	83.9	297.1	343.8	2.9	0.86	0.24	0.62

Table 1: Table of the flight parameters with the engine primary shaft speed N1 in percent, the flight speed U_f , the jet nozzle exit speed U_j in m/s, the speed of sound a at the flight level, the wind speed U_w in knots, and the jet, flight, and relative Mach numbers.

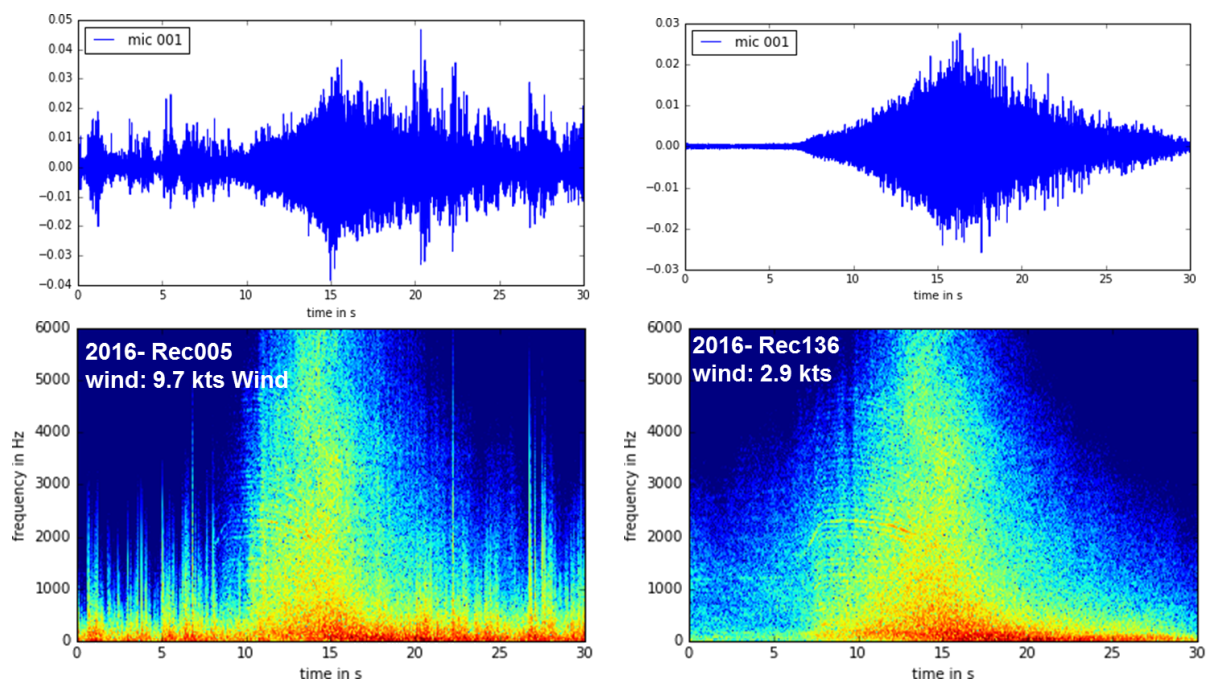


Figure 3: Time series and spectrograms of one microphone in the centre of the array for flyovers REC005 and REC136 in the take-off configuration illustrating the impact of relatively high and low wind during the measurement.

For this paper, fly-overs in the take-off condition were selected from the large database acquired during the 2016 LNATRA fly-over tests. The parameters of the fly-overs presented here are listed in table 1. The engine shaft speed N1 and the flight speed U_f were extracted from the aircraft flight logs for the time when the aircraft was over the array together with the static and total temperatures, which were used to calculate the speed of sound. These parameters were used as input into the numerical performance model at the DLR department AT-TWK, who calculated the jet speed at the engine nozzle. The wind speed and direction were measured with a meteorological station on a 5 m mast about 300 m away from the microphone array. During the fly-overs in the take-off configurations presented here, the aircraft passed the array at altitudes

between 160 and 190 m at the position that corresponds to an emission angle of $\theta = 90^\circ$.

The experimental conditions for fly-over tests are difficult especially due to weather conditions. The certification conditions that are defined in the ICAO Annex 16 document [2] restrict acoustic measurements in several ways in order to avoid a degradation of the results by wind or atmospheric absorption effects. The wind limits prescribed in ICAO Annex 16 are 12 kts for wind in the direction of flight and 7 kts for crosswind. Figure 3 shows the time series and the spectrograms of a single microphone in the centre of the array for two fly-overs in the take-off condition from measurements on two different days. In the first, REC005, the wind speed was 9.7 kts in the direction of flight, in the second, REC136, only 2.9 knots in the cross-wind direction. Compared to REC005, the results from REC136 are relatively clean. The higher wind, which is still well below the ICAO limit, adds low-frequency, random noise to the data. The wind noise, however is local at the microphones and only locally correlated over a smaller area. The focussing of the array onto the aircraft combined with a spatial weighting that reduces density of microphones from the centre of the array reduces the influence of the wind for low frequencies.

For all these fly-overs, the landing gear was retracted and the slats and flaps of the wing high-lift system were set to the Flaps 3 configuration ($22^\circ/20^\circ$). The table presents a selection of four fly-overs in three different take-off configurations. In configuration 1, the nominal conditions are an engine primary shaft speed in the cut-back condition with $N1=80\%$ and a flight Mach number of $M_f = 0.2$. Configuration 2 is a take-off with nominally $N1=91\%$ and $M_f = 0.2$, and configuration 3, again, cut-back with $N1=80\%$ but a higher flight speed with $M_f = 0.25$.

3 Data analysis

For the evaluation of the microphone data, the flight trajectory was estimated from the laser trigger signals and the flight log of the aircraft. The flight log data was also used to determine the pitch, yaw, and roll angles to align the interrogation grid for the beamforming analysis with the aircraft.

The data were analysed with a resampling frequency of 23.5 kHz in the frequency range of the one-third-octave bands between 100 Hz and 10 kHz. The data are analysed in time intervals of the data that correspond to emission angles $\theta = 60^\circ$, 90° , and 120° between the centre of the array and the aircraft axis. These angles are representative of positions when the aircraft is approaching the array, when it is above the array, and when it flies away from it, respectively. The analysis is performed over an interval of $\Delta\theta \pm 5^\circ$. With the flight velocity and the height of around 300 m above the array, this corresponds to only about 10000 samples, or 0.2 seconds of data.

The data were analysed by synchronising the trajectory data with the microphone time records. The method is similar to that described in Siller et al. [8]. In a first pass, the classical beamforming for moving sources [6] that is implemented in the DLR PRoSigMA code was applied. The resulting source maps were used to adjust the trajectory and properly centre the aircraft in the interrogation grid. Such corrections are necessary in order to compensate uncertainties in the trajectory data and deviations from a straight propagation path between the microphones and the aircraft due to wind or thermal variations with height. After the corrections of the trajectory, the proper source localisation was performed with the hybrid deconvolution in ProSigMA [1] in order to calculate source maps in one-third-octave bands on the interrogation

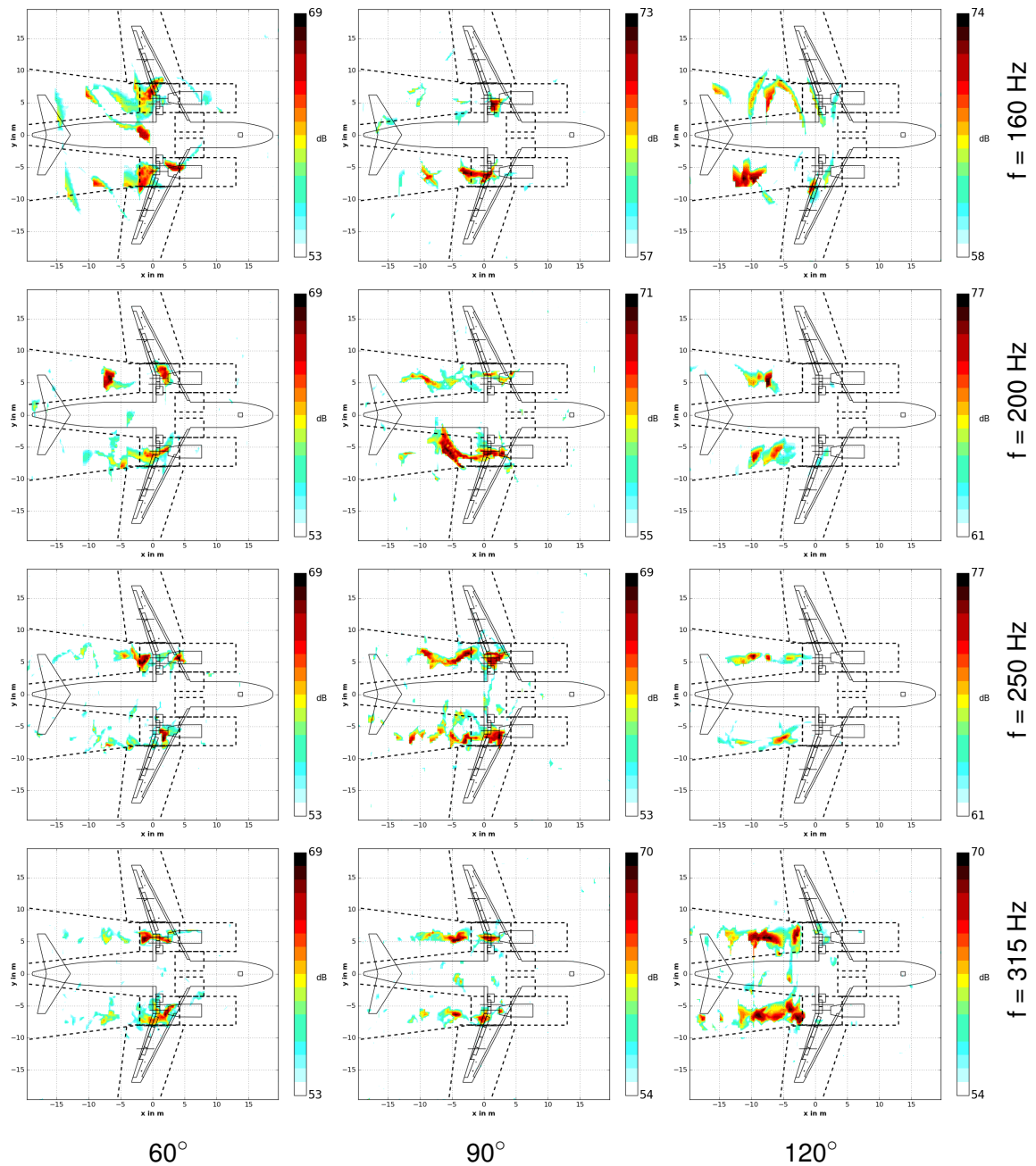


Figure 4: Source maps for the TOBs between 160 and 315 Hz for flyover REC136.

grid that moves with the aircraft.

In the post-processing of the results, the interrogation grid for the calculation was divided into source regions. For the analysis of the jet noise these were the areas around the engine inlet, the nozzle, and the jet region downstream. The source powers in these regions can then be compared on the basis of one-third-octave spectra. With a proper scaling of the sound powers with the flight speed, the altitude, the jet speed, e.g. as proposed by Michel [5], and a compensation

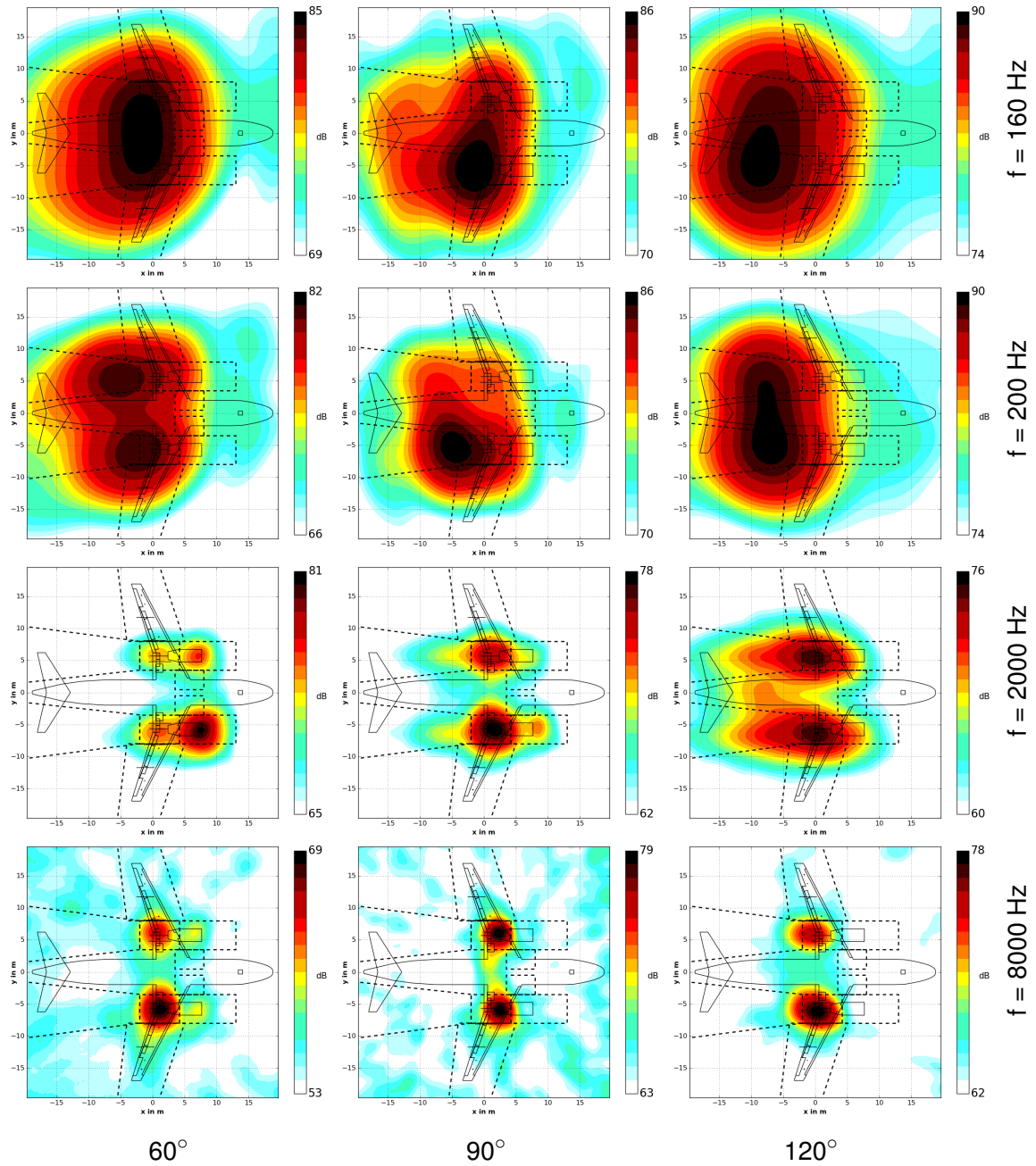


Figure 5: Classical beamforming maps for the 160, 200, 2000, and 8000 Hz bands for flyover REC136.

of the atmospheric absorption of sound, the results of different fly-overs can be averaged and compared.

The data presented here, however, are only scaled to a common reference height of 120 m because the sound power levels of the different fly-overs in the same configurations turned out to be very repeatable so that a scaling on jet and flight speed parameters did not improve the

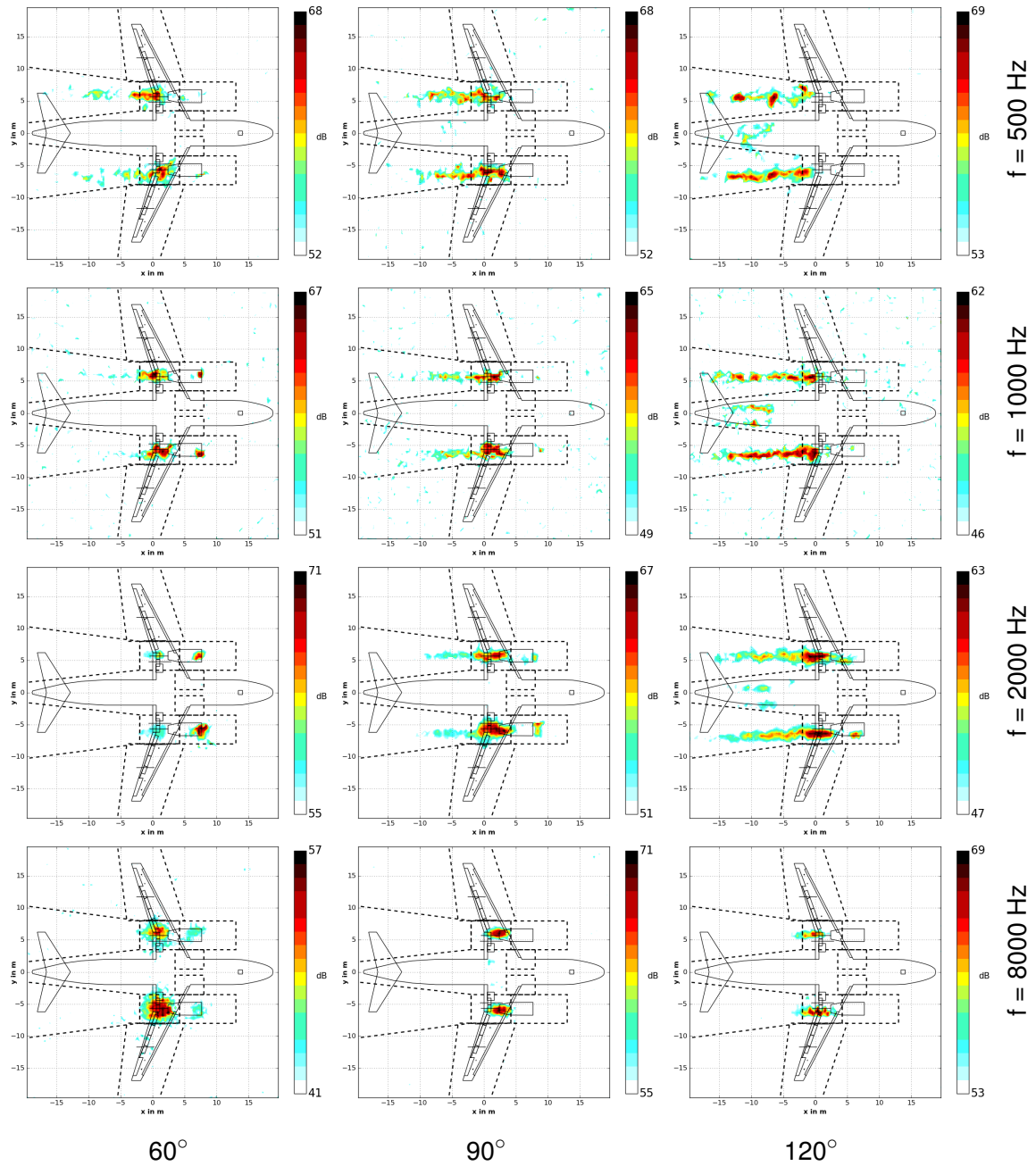


Figure 6: Source maps for the TOBs with 500 Hz and 1 kHz, the 2 kHz band with the fan BPF, and the 8 kHz band with the turbine tones for flyover REC136.

comparison of different fly-overs. In order to compensate the different atmospheric absorption conditions due to different temperature and humidity, the sound pressure levels are rescaled according to the ACSA method, which first restores the levels under lossless conditions and subsequently rescales them to the ICAO standard conditions as described in ISO 9613-1, Attenuation of Sound During Propagation Outdoors [3].

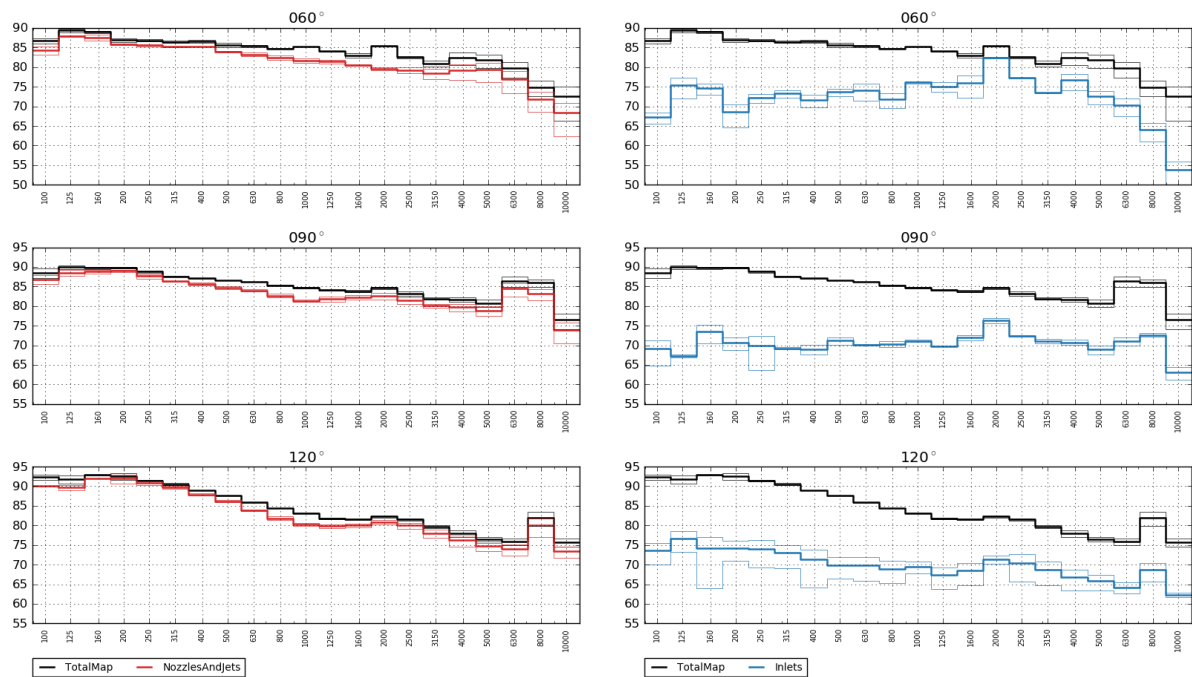


Figure 7: Configuration 2: frequency spectra of the integrated source powers over the whole map area (Total Map) and in the left-hand side graph the combined source regions of the jets and nozzle regions, in the right-hand side graph the engine inlet regions for the two fly-overs REC005 ($N1=90.6\%$ and 77.6 m/s and high wind) and REC 136 ($N1=90.0\%$ and 67.2 m/s). The thicker solid lines indicate the average of the two fly-overs, the thin lines the individual results.

The source maps are calculated on a grid of 40 by 40 m with 99 by 99 grid points with a spatial distance of 0.4 m. The spectral analysis is performed with a Hann window of 2048 samples.

The analysis of all flyovers shows a good repeatability of the results in one configuration. So one typical fly-over per configuration was chosen. In configuration 2, two fly-overs were selected, one which was measured under less favourable weather conditions with significantly higher wind speed, which degrades the microphone data by uncorrelated low frequency noise.

Figure 4 presents sound source maps from the deconvolution analysis in the lowest frequency bands. The 160 Hz band shows spurious noise sources that do not really seem to correspond to features in the engine jets. The 200 Hz band seems to be the practical limit for an analysis over an angular range of $\Delta\theta \pm 5^\circ$ under these flight conditions. From the 200 Hz band on to higher frequencies, the most prominent features in the source maps are sources at the engine nozzles and in the jet region.

For higher frequencies, see figure 6, the jet sources remain visible, in the maps for the 500 and 1000 Hz bands even in the forward arc. In the rear arc with $\theta = 120^\circ$, sources appear on the fuselage far downstream of the engines. These could be reflections, interaction between the jet and the fuselage, or boundary layer noise on the fuselage. The 2 kHz band contains the blade passing frequency (BPF) of the fan (which is at 1865 Hz), and the 8 kHz band contains the tones

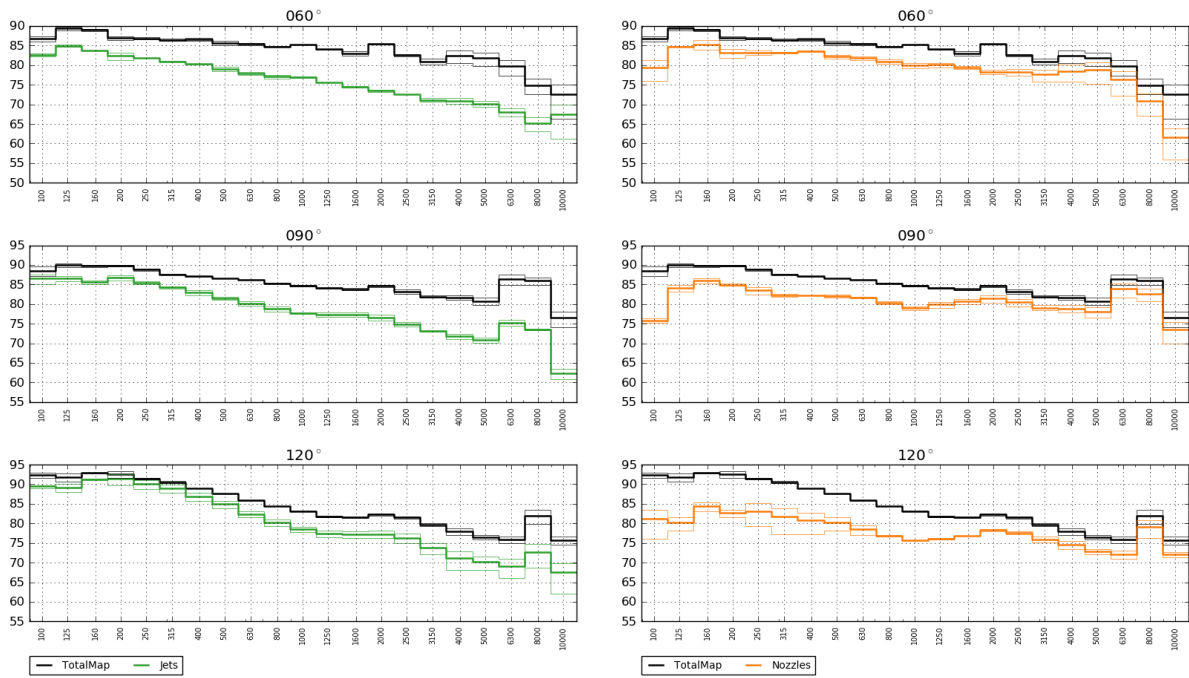


Figure 8: Configuration 2: frequency spectra of the integrated source powers over the whole map area (Total Map) and in the left-hand side graph the jet regions, in the right-hand side graph the engine nozzle regions for the two fly-overs REC005 ($N1=90.6\%$ and 77.6 m/s and high wind) and REC 136 ($N1=90.0\%$ and 67.2 m/s). The thicker solid lines indicate the average of the two fly-overs, the thin lines the individual results.

generated in the last stages of the low pressure turbines. The deconvolution maps retain a high dynamic range up to 8 kHz and above.

Interestingly, the source maps calculated with the classical beamforming algorithm for moving sources, see figure 5, show rather well behaved images – however with a large beamwidth and useless for a quantitative analysis for distributed sources in the jet regions. In the 160 Hz band, the beamwidth of the beamforming maps is about 5 metres wide but indicates the strongest sources at the engine nozzles in the forward arc ($\theta = 60^\circ$) and overhead ($\theta = 90^\circ$), but about 5 m further downstream of the wing trailing edge for $\theta = 120^\circ$. The deconvolution solution in these very low frequency bands is not able to provide a clear localisation of sources and the images are difficult to interpret. In the higher frequency bands, the beamwidth decreases. The beamforming maps in the higher frequency bands, for 2 and 8 kHz (in the two lower rows of graphs in figure 5), show that the spatial weighting of the microphones ensures a relatively constant beamwidth, which had been the original design criterion. In the very high frequency bands, here for 8 kHz, the dynamic range is reduced.

This qualitative inspection of the sound source maps gives very similar results for fly-overs in the three configurations that are presented here. However, the source maps emphasize the point sources. In the take-off configurations presented here, however, most of the acoustic energy comes from the distributed sound sources in the engine jets. The contribution of distributed sources can only be quantified by integrating the source powers. For this purpose, the source

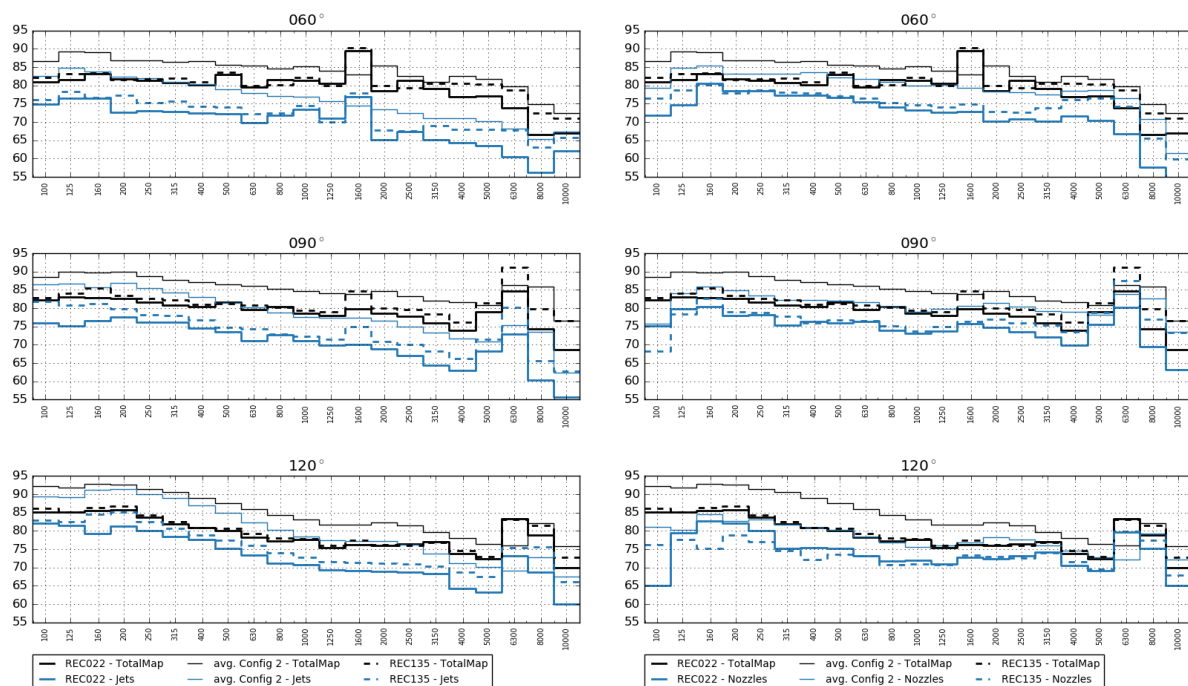


Figure 9: Frequency spectra of the integrated source powers over the whole map area (Total Map) and on the left-hand side the jet noise region, on the right-hand side the nozzle region for fly-over REC135 in configuration 1, the averaged powers from configuration 2 (see figures 7 and 8), and fly-over REC022 for configuration 3.

regions that are indicated as dashed lines in the source maps were defined. Grid points inside these regions were used for the integration over source regions for the engine inlets, nozzles, the jet, the slat horn region at the roots of the wings, and the wings. A very precise spatial analysis of source locations is not possible because of the difficulties involved in precisely tracking the aircraft and aligning the calculated sources with the aircraft. This analysis, however, cannot provide very detailed information, for example to separate the contribution from the engine nozzle from that of jet-flap interaction noise. But it can be very useful in comparing different flight configurations or the acoustic effects of modifications to an aircraft.

In order to compare the contributions of the different source regions, they are compared to the total energy contained in the whole map region.

Figure 7 shows the frequency spectra of the integrated source regions of the combined nozzle and jet regions and the inlet region for the two fly-overs in configuration 2 (REC005 and REC136) compared to the total power integrated over the whole map. The average of the two fly-overs is indicated by a thick solid line, the individual fly-overs by thin lines.

The match between the two individual fly-overs is very good. The sources contained in the combined jet and nozzle regions are the dominating sound sources in the low frequency range. The sources at the engine inlet are less prominent, except for the BPF tone at 2 kHz at $\theta = 60^\circ$ and 90° . When the source regions are separated between the jet and the nozzle, where the border is more or less arbitrarily chosen, the jet sources have a maximum between 125 and 200 Hz and decrease for higher frequencies. For $\theta = 90^\circ$ and 120° , the turbines tones also show up in

the jet noise region. The nozzle sources are closer to the total energy in the maps for higher frequencies, which can be explained by the evolution of structures in a turbulent jet which starts with small scales and evolves to increasingly larger structures which generate lower frequency noise in the downstream direction.

The different contamination of the raw data with wind between flyover REC005 and REC136 does not seem to have a significant influence on the deconvolution results. The focussing of the array onto the aircraft seems to be able to suppress the local effects of wind on the microphone signals.

Figure 9 presents results of all three configurations, REC135 in configuration 1 in dashed lines, the average of configuration 2 in thin solid lines, and REC022 in configuration 3 in thick solid lines. Configuration 2 with the highest relative jet Mach number $M_j - M_f$ (see table 1) is the loudest. The level differences between config 1 and 3 is relatively small, just like the differences between their relative Mach numbers. The most striking feature, however, is that for configs 1 and 3 the levels in the 1.6 kHz band that contains the BPF noise are higher than in the 2.0 kHz band of configuration 2 that contains the BPF for the higher shaft speed in configuration 2. Flyover REC135 in configuration is a couple of dBs louder in the jet noise, because the higher flight speed reduces the relative Mach number $M_j - M_f$, which is the critical parameter of the jet noise.

4 Conclusions

The analysis of different fly-overs in the take-off configuration shows that the contribution of jet noise can be analysed quantitatively from array measurements. Apart from the difficulties of performing fly-over measurements with large arrays, the largest constraint on the data analysis is the resolution of sources at very low frequencies, where both jet-noise and wind influence on the microphones are great. Due to the short time slots of the fly-over segments for the emission angles 60° , 90° , and 120° with an interval of $\Delta\theta = \pm 5^\circ$, the averaging of the results in the low frequency one-third-octave bands is rather poor. The comparison of results from flyovers in the same configuration but on different days, one with low, the other with relatively high wind speed, shows that the results are well reproduced and the contamination of the signal by wind on the microphones does not influence the results. The focussing of the array on the aircraft together with the large spatial extent of the array seem to work together to reduce the local effect of low-frequency wind noise on the microphones.

Acknowledgements

This project has received funding from the Clean Sky 2 Joint Undertaking under the European Union's Horizon 2020 research and innovation programme under the grant agreement Number 807097 - LPA GAM 2018 - H2020 – IBA - CS2 - GAMS - 2017.



The authors thank Florian Wolters from DLR AT-TWK in Cologne for providing the nozzle exit speeds of the V2500 engine with a numerical code.

REFERENCES

- [1] S. Guérin and C. Weckmüller. “Frequency-domain reconstruction of the point-spread function for moving sources.” In *Proceedings on CD of the 2nd Berlin Beamforming Conference, 19-20 February, 2008*. GfAI, Gesellschaft zu Förderung angewandter Informatik e.V., Berlin, 2008. ISBN 978-3-00-023849-9. URL http://www.bebec.eu/Downloads/BeBeC2008/Papers/BeBeC-2008-14_Guerin_Weckmueller.pdf.
- [2] International Civil Aviation Organisation (ICAO). *International standards and recommended practices. Environmental protection. Annex 16 to the convention on international civil aviation*, volume I, 2nd edition. International Civil Aviation Organisation (ICAO), 1988.
- [3] ISO 9613-1. *Acoustics: Attenuation of sound during propagation outdoors*. International Organisation for Standardisation (ISO), Geneva, Switzerland, 1993.
- [4] W. R. Krüger, F. Boden, T. Kirmse, J. Lemarechal, A. Schröder, H. P. Barth, S. Oertwig, H. Siller, J. W. Delfs, A. Moreau, D. Schäfer, A. Stürmer, and M. Norambuena. “Common numerical methods & common experimental means for the demonstrators of the large passenger aircraft platforms.” In *Aerospace Europe Conference 2020*. 2020. URL <https://elib.dlr.de/133985/>.
- [5] U. Michel. *Prediction of jet mixing noise in flight from static tests*. 2016. doi:10.2514/6.2016-2807. URL <https://arc.aiaa.org/doi/abs/10.2514/6.2016-2807>.
- [6] J.-F. Piet, U. Michel, and P. Böhning. “Localization of the acoustic sources of the A340 with a large phased microphone array during flight tests.” In *8th AIAA/CEAS Aeroacoustics Conference, Breckenridge, Co, 17-19 June 2002*. 2002. URL http://pdf.aiaa.org/preview/CDReadyMAERO02_554/PV2002_2506.pdf.
- [7] Siller, Hage, and Schumacher. “Source localisation on aircraft in flight - new measurements with the dlr research aircraft airbus 320 atra.” In *Proceedings on CD of the 7th Berlin Beamforming Conference, March 5-6, 2018*. GfAI, Gesellschaft zu Förderung angewandter Informatik e.V., Berlin, 2018. ISBN 978-3-942709-20-0. URL <http://www.bebec.eu/Downloads/BeBeC2018/Papers/BeBeC-2018-D01.pdf>.
- [8] H. Siller. “Localisation of sound sources on aircraft in flight.” In *Proceedings on CD of the 4th Berlin Beamforming Conference, 22-23 February 2012*. GfAI, Gesellschaft zu Förderung angewandter Informatik e.V., Berlin, 2012. ISBN 978-3-942709-04-0. URL <http://bebec.eu/Downloads/BeBeC2012/Papers/BeBeC-2012-01.pdf>.